Biophotonics Congress: Biomedical Optics Congress 2018 (Microscopy/Translational/Brain/OTS) © OSA 2018

How Should the New Generation of Detectors for Diffuse Optics Be? A Systematic Simulation Study

Laura Di Sieno[1], Anurag Behera[1], Antonio Pifferi[1,2], Fabrizio Martelli[3], Alberto Dalla Mora[1]
[1] *Politecnico di Milano, Dipartimento di Fisica, Piazza Leonardo da Vinci 32, 20133 Milano, Italy*
[2] *Consiglio Nazionale delle Ricerche, Istituto di Fotonica e Nanotecnologie, Piazza Leonardo da Vinci 32, 20133 Milano, Italy*
[3] *Università degli Studi di Firenze, Dipartimento di Fisica e Astronomia, Via G. Sansone 1, 50019 Sesto Fiorentino, Firenze, Italy*

Author e-mail address: laura.disieno@polimi.it

Abstract: In this work we report a comprehensive simulation study in which we quantify the effects of all parameters affecting the Instrument Response Function of a time-domain system in terms of sensitivity to an optical perturbation.
OCIS codes: (110.7050) Turbid media; (300.6500) Spectroscopy, time resolved; (170.5280) Photon migration; (170.3660) Light propagation in tissue.

1. Introduction

In the last few years great improvements in the systems for time-domain (TD) diffuse optics (DO) have been made. Indeed, the use of Silicon Photo-Multipliers (SiPM) [1,2] along with new compact pulsed laser sources [3] has opened the way to a new generation of instruments characterized by lower dimension and price with respect to classical instrumentation. However, the realization of wearable devices and the achievement of the ultimate performances from time-domain technique can bring the TD-DO instruments to a widespread use, exploiting the intrinsic advantages of the TD acquisitions (capability to disentangle reduced scattering coefficient from absorption one, depth encoded in the arrival time of photons). To achieve both aims, it has been demonstrated that a dense grid of fast time-gated (~100 ps) detectors to maximize the photon collection area (~1 cm^2) is required, along with many laser injection points to maximize the amount of light injected into the sample. For what concerns the detector, the recent introduction of SiPMs in diffuse optics opens the way to new scenarios. Indeed, the SiPM allows us to increase significantly the overall light harvesting of the system (due to their relatively large area –about 1 mm^2– and the possibility of placing them directly in contact with the sample/tissue [4]) . Additionally, with the use of a CMOS process it is possible to have the read-out electronics embedded along with the detector thus making the SiPMs good candidates for the new generation devices. However, the long tails in the Instrument Response Function –IRF– (see [5] for details) and the relatively high dark count rate, set a limit to the maximum achievable dynamic range thus limiting the maximum penetration depth. Moreover, at present they can not be fastly time-gated (i.e. it is not possible to turn them on within few tens of ps). Thus it is not possible to exploit the small source-detector separation approach which leads to increased contrast at any time and improved spatial resolution. It is clear that the careful design of the new generation detectors and sources is of the utmost importance to devise wearable and dense devices. In this work we present a comprehensive simulation study in which the effect of all parameters affecting the IRF (diffusion tails, light harvesting defined by the responsivity parameter, full-width at half maximum –FWHM–, noise sources such as dark count rate –DCR–) are studied depending on the geometrical (position and size of the optical perturbation to be detected) and optical (background optical properties and the amount of the optical perturbation with respect to the background) conditions. For this reason, the study has a dual aim: i) drive further the technological development of the new generation TD-instrument; ii) for a given technology (i.e. given IRF) and optical/geometrical conditions, to provide scientists a guide to choose the best measurements conditions (e.g. interfiber distance).

2. Material and method

In this work we made use of an 8th-order perturbative solution of the Transport Equation under the Diffusion approximation along with Extrapolated Boundary conditions [6]. To take into account the effect of different systems (i.e. different characteristics of laser and detector) we convolved the theoretical distribution of time-of-flight (DTOF) with the IRF. Additionally, we simulated the effect of time gating by slicing the DTOF curves before applying any count rate limitation to mimic real measurements. For what concerns the noise, we added both a constant value (i.e. dark count noise which is a peculiar characteristic of a detector) as well as the shot noise.
The simulator has been built using an external framework (written in Matlab®) with 4 iterators. Such a solution allows us to change different parameters (e.g. background optical properties, absorption perturbation, features of the IRF, location of the inhomogeneity, …). On the other hand, the simulation of both perturbed and homogeneous DTOF was done by a central kernel compiled in C for increase computational efficiency.

To objectively compare the performances achieved with different features of the IRF, we made use of two well-assessed figures of merit (defined in the nEUROPt protocol [7]): contrast and contrast-to-noise ratio (CNR). In both cases, we used the "time windowing" (i.e. each DTOF acquisition was divided into portions called "gate", t_g) of the curve. The gate width was set 500 ps and its position was referred to the peak of the IRF. In eq. (1a) and (1b) are reported the definition of contrast and CNR:

$$C(t_g) = \frac{N_0(t_g) - N(t_g)}{N_0(t_g)} \quad (1a); \qquad CNR(t_g) = \frac{N_0(t_g) - N(t_g)}{\sigma(N_0(t_g))} \quad (1b)$$

where $N_0(t_g)$ and $N(t_g)$ are the number of counts in the unperturbed (i.e. homogeneous) and perturbed (i.e. heterogeneous) state respectively while $\sigma(N_0(t_g))$ is the photonic noise (i.e. $\sqrt{N_0(t_g)}$).

3. Results and discussion

For the purpose of brevity, in the present abstract we will show only the results obtained for an IRF of a state of the art setup [8] characterized by: i) Full-Width Half-Maximum of 150 ps; ii) DCR of 100 kcps; iii) injected power on the sample: 60 mW; iv) responsivity of $3.014 \cdot 10^{-11}$ m^{2}sr (typical of the state-of-the-art fast time-gated system based on 100 µm diameter SPAD [9]); v) wavelength: 820 nm; vi) first diffusion tail with time constant of 80 ps.

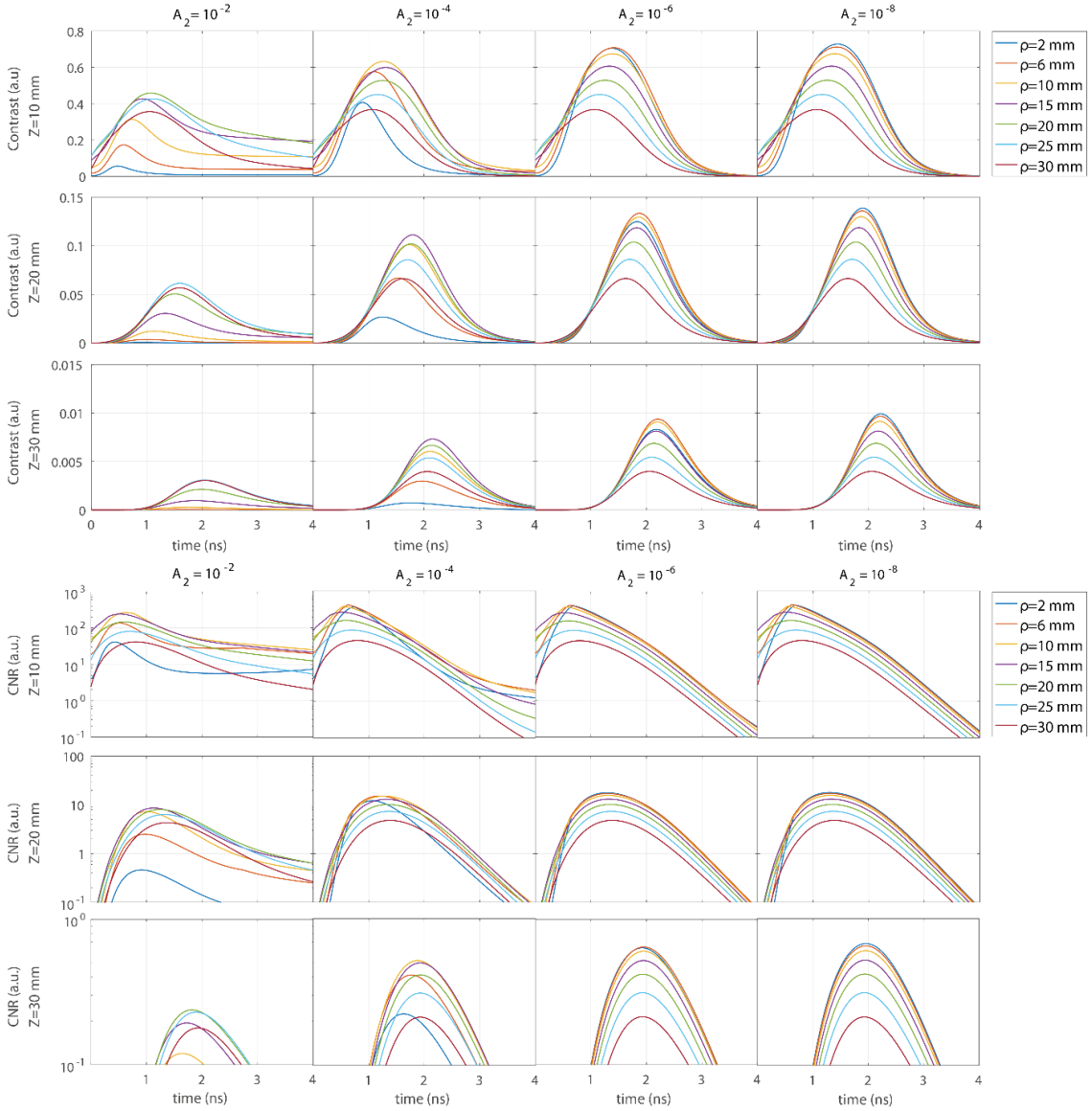

Fig. 1. Contrast (top graphs) and CNR (bottom graphs) computed for different SDS (colors) at 3 depths (rows) simulating IRF with amplitude of the second slow tail amplitude (A_2) varying from 10^{-2} to 10^{-8} with respect to the IRF peak (columns).

For what concerns the optical/geometrical conditions we used a standard background (μ_a= 0.1 cm^{-1} and μ_s'= 10 cm^{-1}) in which an absorbing perturbation ($\Delta\mu_a$= 0.162 cm^{-1}) was buried at variable depth (10, 20 and 30 mm). In this case, the feature of the IRF is mostly due to the detector response.

Figure 1 reports the results (contrast and CNR, top and bottom respectively) were obtained by changing the amplitude of the second slowly decaying diffusion tail -i.e. the so-called memory effect [10]- (columns) at different depths of the inclusion (rows). The amplitude value of the second diffusion tail (time constant: 1.8 ns) has been set to 2, 4, 6 and 8 decades below the IRF. Both contrast and CNR are shown for different source-detector separation (SDS) ranging from 2 to 30 mm.

For contrast, it is evident that, at all depths, the smaller SDS (2 mm) is not the best choice, for tail amplitude of 2 and 4 decades, where the maximum contrast can be achieved using larger SDS (10 mm for all depths for A_2= 10^{-4} while for A_2 = 10^{-2} even larger values -20 or 30 mm- are better). On the other hand, if the dynamic range of the IRF is increased (i.e. A_2= 10^{-6} and A_2 = 10^{-8}) better performances are obtained with smaller SDS (6 mm).

For what concerns the CNR, for inclusion shallower than 3 cm, the best results are generally obtained for SDS of 10 mm (which has higher CNR for lower time). Only for the IRF with A_2=10^{-2} the results are less clear, with the best SDS for depth of 10 and 20 mm inclusion depth being the 10/15 and 15/20 mm. If the perturbation is buried 3 cm below the surface, the higher the second tail amplitude, larger has to be the SDS to get the maximum CNR. Indeed, the highest CNR and contrast are obtained for SDS equal to 20, 10, 6 and 2 for A_2 equal to 10^{-2}, 10^{-4}, 10^{-6} and 10^{-8} respectively. However, it has to be noted the CNR is lower than 1 for all SDS, meaning that the inclusion is not detectable (limit for detectability: CNR = 1 meaning that the contrast is comparable with the measurement noise). However, such a problem could be solved using a system with larger responsivity (i.e. replacing the fast-gated SPAD with a larger area detector as a SiPM).

4. Conclusions

We realized a simulation software which allows to i) give to scientists the best experimental conditions (e.g. choice of the SDS for a given system (IRF) and optical problem); ii) to devise the new generation of detectors for diffuse optical system. Moreover, we understood that the choice of the SDS to achieve better contrast and signal is strongly dependent on the IRF features of the system, such as the amplitude of the second slow diffusion tail (A_2). Indeed, for A_2>10^{-4} the use of the null-source detector separation is no more the best option, despite the prediction done by theory. Such a finding implies the careful layout of new detector where the layers have to be designed to decrease the effect of such a diffusion tail. Other strong dependencies of contrast and CNR from IRF features (responsivity, DCR and FWHM) can be inferred using the proposed software. Just as an example, the effect of the FWHM is negligible for value lower than 150 ps while the effect of the overall light harvesting of the system is affecting the CNR which increases almost linearly with the responsivity.

5. Acknowledgments

This project has received funding from the European Union's Horizon 2020 research and innovation programme under grant agreement no 654148 Laserlab-Europe; no 675332 BitMap and no 731877 SOLUS: Smart OpticaL and UltraSound diagnostics of breast cancer.

6. References

[1] A. Dalla Mora et al, "Fast silicon photomultiplier improves signal harvesting and reduces complexity in time-domain diffuse optics," Opt. Express **23**, 13937–13946 (2015).
[2] A. Pifferi et al, "New frontiers in time-domain diffuse optics, a review," J. Biomed. Opt. **21**, 91310 (2016).
[3] L. Di Sieno et al, "Miniaturized pulsed laser source for time-domain diffuse optics routes to wearable devices," J. Biomed. Opt. **22**, 85004 (2017).
[4] R. Re et al, "Probe-hosted silicon photomultipliers for time-domain functional near-infrared spectroscopy: phantom and in vivo tests," Neurophotonics **3**, 45004 (2016).
[5] E. Martinenghi et al, "Spectrally-resolved single-photon timing of silicon photomultipliers for time-domain diffuse optics," Photonics Journal, IEEE **7**, (2015).
[6] A. Sassaroli et al, "Forward solvers for photon migration in the presence of highly and totally absorbing objects embedded inside diffusive media," J. Opt. Soc. Am. A **31**, 460 (2014).
[7] H. Wabnitz et al, "Performance assessment of time-domain optical brain imagers, part 2: nEUROPt protocol," J. Biomed. Opt. **19**, 86012 (2014).
[8] L. Di Sieno et al, "Functional near-infrared spectroscopy at small source-detector distance by means of high dynamic-range fast-gated SPAD acquisitions: First in-vivo measurements," Proc. SPIE - Int. Soc. Opt. Eng. 880402–880406 (2013).
[9] L. Di Sieno et al, "Characterization of a time-resolved non-contact scanning diffuse optical imaging system exploiting fast-gated single-photon avalanche diode detection," Rev. Sci. Instrum. **87**, (2016).
[10] A. Dalla Mora et al, "Memory effect in silicon time-gated single-photon avalanche diodes," J. Appl. Phys. **117**, 114501 (2015).